Development and Application of In Situ High-Temperature, High-Pressure Magic Angle Spinning NMR

Nicholas R. Jaegers, Mary Y. Hu, David W. Hoyt, Yong Wang, and Jian Zhi Hu

Abstract

Solid-state NMR has served as an important tool for investigating chemical systems, not only to better understand the structure of materials, but also to probe the interactions that occur between two or more constituents. Disparities between realistic chemical environments and those experienced during spectroscopic measurements have challenged a firm understanding of these systems. To address this concern, novel methods of conducting NMR spectroscopy under conditions of high pressure and high temperature have been developed to simulate these harsh conditions. Herein, the advancement of this technology is described by detailing the design iterations as the methods have matured to their present state. Several applications from the fields of geochemistry, catalysis, and materials science are recounted that demonstrate the capabilities and usefulness of high-temperature, high-pressure MAS NMR across diverse facets of scientific study.

Keywords

In situ NMR • High-pressure • High-temperature • Geochemistry • Zeolite • Biomass • Material synthesis

N.R. Jaegers • Y. Wang
Pacific Northwest National Laboratory, Institute for Integrated Catalysis and Earth and Biological Science Directorate, Richland, WA, USA

Voiland School of Chemical Engineering and Bioengineering, Washington State University, Pullman, WA, USA

M.Y. Hu • D.W. Hoyt • J.Z. Hu (✉)
Pacific Northwest National Laboratory, Institute for Integrated Catalysis and Earth and Biological Science Directorate, Richland, WA, USA
e-mail: jianzhi.hu@pnnl.gov

G.A. Webb (ed.), *Modern Magnetic Resonance*,
https://doi.org/10.1007/978-3-319-28275-6_93-1

Contents

Introduction – A Historical Perspective

Fundamental studies on chemical systems intensively utilize spectroscopic methods to provide thorough insight on the subject of interest. Often, the desire is to observe these systems under the conditions at which the reactive transformations take place. The importance of observing detailed structural and dynamic information under nondestructive, realistic reaction conditions has promoted the development of NMR methods capable of withstanding much harsher conditions than traditional NMR technologies. While the development of magic angle spinning (MAS) NMR has significantly enhanced the quality of information obtained from solid samples, methods that allowed for internal high-pressure environments were not reported for decades after the development of MAS [1, 2]. This shortfall hindered studies that are sensitive to environmental effects. Many catalytic systems, for example, operate at elevated temperatures and pressures where unique chemical species do not exist at more mild conditions. Given the importance of mirroring these more drastic conditions, a critical need was identified for developing in situ MAS NMR techniques to provide relevant spectroscopic information that would not otherwise be available.

A number of technical challenges impeded early advancement of methods that allowed for spectroscopic observation under high-temperature, high-pressure conditions. In particular, the material of the NMR rotor has to withstand the conditions present within its walls as it rotates at several kilohertz. Metallic sample cells are unusable due to the powerful eddy currents generated by spinning metal in a strong magnetic field, limiting the construction to materials such as glasses, ceramics, and plastics. Early work in the late 1990s and early 2000s utilized flame or epoxy-sealed Pyrex tubes inserted into traditional spinners to investigate the segmental motion of polymers plasticized by dense gases [3–5]. This format experienced challenges in exceeding 70 bar due to the fragility of the glass. Furthermore, it was impossible to reuse or open the sample cell if additional material was to be introduced, limiting the applications and encouraging the development of technologies based on other materials.

PEEK™ and Delrin™ polymer-based inserts fitted inside a regular high-mechanical strength ceramic rotor sleeve also had success up to 70 bar, but dramatic chemical penetration of CO_2, N_2O, and CH_3F into the polymer material was evident, which decreased the pressure over time [6, 7]. Deuchande et al. also encountered further limitations in the pressure (40 bar) when spinning up to several kilohertz due

to the difficulties in constructing a secure, high-pressure sealing mechanism on smaller rotors. These rotors also suffered from severe carbon and proton background signals that severely complicated analysis of the nuclei in samples. The described drawbacks of glass- and polymer-based NMR rotors have led to the utilization of ceramic materials for high-temperature, high-pressure (HTHP) applications of MAS NMR. Herein, we describe the recent development of such technologies and the applications for which these advanced methods have more completely described the chemical systems.

Recent Technological Advances

Bearing attention towards the drawbacks of metallic, glass, and plastic rotor materials, ceramic-based designs are attractive for their high mechanical strength and common use in MAS NMR, potentially allowing for an extension of pressure far beyond the previously observed limit of 70 bar. The first high-pressure, MAS-capable ceramic design utilized commercial NMR rotors fit with custom components [8]. As shown in Fig. 1a, standard ceramic zirconia sleeves (1) and commercial drive tips (e.g., Kel-F or Vespel) (2) were fit together. Internally, the sleeve walls outside of the sample space were roughened and an epoxy was applied to tightly bind the PEEK bushings (4 and 5) to the interior surface of the sleeve. A removable TORLON plug (7) and valve adapter (6) were threaded into the bushings on each side and sealed with O-rings. Finally, the sample cell was sealed by inserting the TORLON valve (8) and threading it into place, a reversible process that allowed for simple recharging of the cell.

The sealing valve for this original model also contained an off-center needle hole to allow for the injection of high-pressure liquids and quick sealing by turning the valve less than one quarter turn without altering the pressure inside the cell. A high-pressure loading chamber accompanied the design to allow for the loading of fluids and subsequent sealing under a high-pressure, controlled environment [8]. The chamber was constructed out of blocks of stainless steel held together by bolts and sealed with an O-ring. The bottom block housed the rotor holding mechanism to maintain immobility during rotor charging and sealing while the top block was constructed to allow for a rotating plug holder to thread the sealing valve into place. The upper block also housed two observation windows and five ports to allow the inflow of gases, two for liquid charging, one for venting, one for thermocouple access, and the last to monitor the system pressure. The internal volume of this chamber was 9 cm^3. The loading system could reach temperatures up to 400 °C and was connected to a piston screw capable of generating pressures of 4,136 bar. The custom-built loading chamber's capabilities were well suited for the experimental needs and exceeded the capabilities of the rotor itself.

Further improvements to the signal were realized given the large sample volume associated with these rotor designs. The original 9.5 mm OD rotor featured a sample volume of 350 μl. Higher pressures could also be realized by this system. Standard zirconia rotors of this size are capable of withstanding pressures up to 486 bar

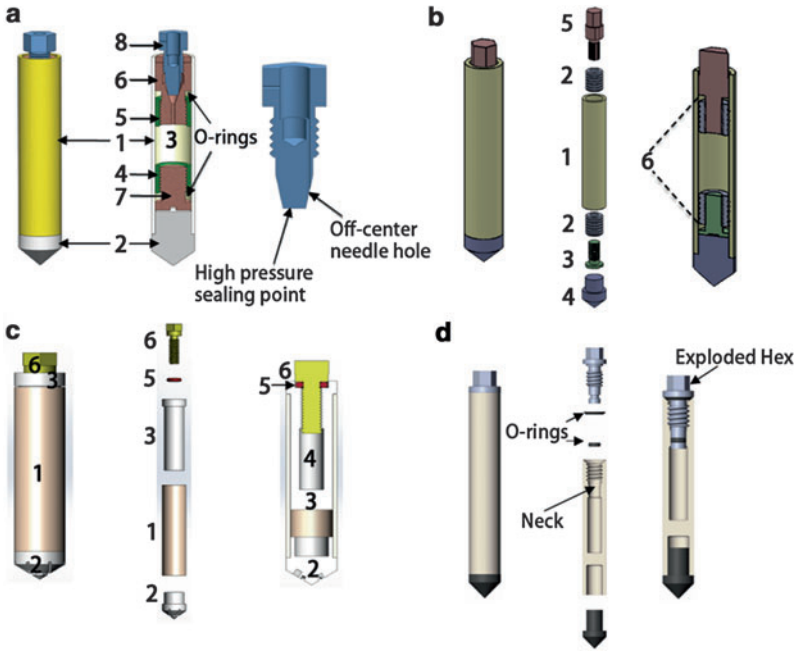

Fig. 1 High-pressure, high-temperature rotors developed for in situ NMR. The first generation (**a**) is shown constructed, with an internal view of the fit and matched components, and an internal perspective of the valve. The modified version of the first generation (**b**) is portrayed constructed, exploded, and with an internal view of the matched/fit components. The second generation (**c**) includes an assembled external view, an exploded interpretation, and an internal depiction. The third generation (**d**) is shown with a constructed depiction, exploded perspective, and an internal view of the fit components. These images are adapted from the Refs. [8] and [9] with permission from Elsevier, Ref. [10] with permission from John Wiley & Sons, and Ref. [11] with permission from The Royal Society of Chemistry

without fracturing. There are two principle contributions to the effective pressure inside the rotor: centrifugal force (F_C) and sample pressure (P_S). These contributions are modeled by Eq. 1:

$$P_T = P_C + P_S = \frac{F_C}{A} + P_S = \frac{\left(R_2^2 - R_1^2\right)^* \rho^* \omega^{2*} R_2}{2^* R_1} + P_S, \tag{1}$$

where R_1 and R_2 are the inner and outer rotor radii, respectively, and ω is the rotational frequency in radians per second. This trade-off between spinning rate and sample pressure allowed for 360 bar of internal pressure spinning at 3.5 kHz before the rotor sleeve would fracture. As such, the TORLON valve adapter, which saw a breaking pressure of 344 bar with test helium charging and demonstrated stable operation at 165 bar and 2.1 kHz with only a 19% loss of pressure over 72 h, was identified as the weakest component.

While the above design highlighted improvements to the state of the art, two design challenges required improvement for widespread application in the research community: the failure point of the valve adapter at high operating pressures and the spinning limitations due to the dynamic relationship between spinning rate and sample pressure, where high pressures severely limit the rotation and cause detrimental peak broadening in the NMR spectra. A second iteration of the first design (Fig. 1b) addressed the former challenge by incorporating sealing plugs (3 and 5) that thread directly into the bushings (2) and compress an O-ring to activate the seal, eliminating the need for the valve adapter [9]. The design also uses a standard 7.5 mm zirconia MAS rotor (1) and spin tip (4) to allow for increased operating pressures at higher spinning rates of up to 200 bar while spinning at 6 kHz, drastically improving the separation of the side bands from center band. The break point for this scheme was again the plastic sealing mechanism. The reiterated design also featured a slightly larger sample volume of 446 μl, which provided a boost to the recorded spectral sensitivity and minimized the gas compression from sealing the cap to just 0.92%. A sizable increase in the sealing was also realized with only a 12.5% reduction in spectral intensity after 90 h of operation. This design was utilized extensively for many of the applications discussed in the subsequent section.

A second generation of rotor design was created to push the limits of operation further. A significant downside to the earlier designs was the temperature limit of 100 °C imposed by degradation of the adhesives at elevated temperatures. This cell is depicted in Fig. 1c. To extend beyond this limitation, a rotor was designed that utilized a commercial 9.5 mm ceramic sleeve (1) and spin tip (2) as before; this time, however, a custom ceramic insert (3) was fitted into the rotor sleeve to form the sample cell [10]. This insert was threaded at the top to allow sealing with a plastic screw (6) pressing down on an O-ring (5) exhibiting high thermal resistance. Due to the use of a high-temperature glue, this new rotor's operational range was extended to 180 °C and 10 bar at 2.4 kHz. While this design certainly improved upon the operational flexibility by way of enhanced temperature resistance and mechanical strength, some drawbacks to the design were noted. Nearly negligibly, the adhesive and the end of the plastic screw fell within the detection area of the RF coil, contributing to background signals in the ^{13}C and ^{1}H channels. Much more impactful was the dramatic reduction in sample volume from previous designs to just 220 μl, increasing acquisition times to four times those required by the previous generation of high-pressure rotors to achieve the same sensitivity.

The inherently iterative nature of technological advance has led to a third major improvement of the previously mentioned rotor designs to address the drawback of sensitivity and continue propelling the technology to more dramatic sample conditions. In the present state of the art, the mechanical strength, chemical resistance, and temperature independence of ceramics are fully utilized to allow for the use of the highest temperature and pressure combinations [11]. In this design (Fig. 1d), all parts except the sealing O-ring and spin tip are constructed of high-mechanical strength ceramics. The rotor sleeve is a ceramic cylinder bored out on the bottom to allow for tight fitting of the spin tip. The other end also contains a cavity, but is not bored through to allow a solid, ceramic barrier between the sample and spin tip spaces. The

top is threaded to allow for a ceramic cap to be securely screwed into the rotor sleeve with a hex where it seals the vessel by pressing an O-ring (or two, depending on the design iteration). This simple design is suitable for a wide range of rotor sizes and has been demonstrated for 9.5 mm, 7.5 mm, 5.0 mm, and 3.2 mm. These rotors house large sample spaces of 430 μl, 300 μl, 75 μl, and 20 μl, respectively, and are suitable for operation at least up to 100 bar and 250 °C, marked increases in operational potential.

These developmental efforts to spectroscopically probe chemical systems under more realistic conditions have widened the boundaries of in situ NMR study towards much higher temperatures and pressures than previously realized. These technologies have progressed from sealed, glass tubes and plastic rotors to more rigid, larger ceramic materials that allow a breadth of reaction conditions suitable for a greater variety of applications. Even over the first few years of development, these technologies have been employed to help solve challenging problems.

Applications

The chemical environment of materials has a dramatic impact on the interactions present in the system, one obvious example being the impacts of temperature and pressure on a catalytic reaction network. When applied judiciously, NMR investigations at high temperatures and pressures have demonstrated great usefulness in understanding systems where reactions take place under harsh conditions. Reported areas where this technology has been utilized are geochemistry, catalysis, and materials synthesis. Herein, we report on the diverse systems for which high-temperature, high-pressure in situ MAS NMR spectroscopy has aided in the understanding of the fundamental chemical interactions. These topics are segmented into the categories listed previously.

Geochemical Interactions

Among the more broadly investigated interactions of small molecules in geological environments, investigating the mineral carbonation reaction mechanisms associated with geological carbon sequestration has become a prominent and widely applied application of the HTHP rotors [12–16]. The storage of carbon in geologic structures remains a promising greenhouse gas mitigation technique owing to the broad abundance of suitable formations. Due to concerns of fluid slippage and a desire for a molecular picture to promote further advances, a solid understanding of the interactions between stored gases and the minerals is important. At depths where sequestration is appropriate, CO_2 is found as a supercritical fluid at 73.8 bar or higher, requiring the use of high-pressure spectroscopy for truly in situ investigation.

An early application of HTHP NMR by Hoyt et al. investigated the catalytic role of water on Mg_2SiO_4 to clarify the metal carbonation reactions taking place [8]. The authors loaded the precisely hydrated mineral into the rotor before charging it with

high-pressure CO_2 (150 bar) at elevated temperatures (50 °C). ^{13}C NMR clearly demonstrated the formation of HCO_3^- species present as a relatively mobile phase (161.5 ppm) at higher pressures. With extended exposure times, a new peak (170.5 ppm) formed, indicating the formation of the carbonation product, magnesite ($MgCO_3$). In the absence of water, Hoyt et al. observed no HCO_3^- species or carbonation reaction, suggesting that water quickly dissolves the carbon dioxide to facilitate mineral carbonation. The more advanced rotor designs later allowed for the ability to conduct the same high-pressure experiments with natural minerals at 150 bar and 6 kHz of spinning, where paramagnetic iron from antigorite induced strong spinning side bands that are only sufficiently separated at high spinning rates [9].

Wollastonite ($CaSiO_3$) was investigated as well to assess the dependence of water content on mineral carbonation up to 160 bar [13]. This study found that silicate minerals are able to undergo extensive carbonation at relatively high water contents in the supercritical CO_2 phase and the extent of carbonation correlated well to higher temperatures and pressures as the solubility of water increased. NMR played a vital role in this study to assess the reactivity under contrasting conditions with both ^{13}C and ^{29}Si NMR showing the extent of carbonate precipitation and amorphous silica species, respectively.

Loring et al. further investigated the influence of water on geologic carbon sequestration, but as it pertained to the sealing of cap rock promoted by the physical expansion of clays [12]. Kaolinite and calcium-rich montmorillonite systems intercalate water and subsequently decrease permeability of the clays as they expand. However, this effect was also seen with the application of only supercritical CO_2 in montmorillonite, as evidenced by significant broadening of the ^{13}C NMR line of CO_2 at 90 bar. In conjunction with other spectroscopic data, this was shown to be a result of the migration of CO_2 into the interlayer, where rotation is constrained and interactions with water are prevented. This effect was not observed in kaolinite, further demonstrating the complexity surrounding the expansion of clay mixtures as a function of environment. Increasing the variety of nuclei probed with the HTHP technique, Bowers et al. investigated the interaction of supercritical CO_2 with Na-hectorite with both ^{13}C and ^{23}Na MAS NMR [14]. The same confinement of supercritical CO_2 was observed in the hectorite system as with montmorillonite where no carbonate species developed, but a rapid site-hopping of sodium cations became evident. The incorporation of an organic compound (humic acid) increased the interlayer incorporation, highlighting the importance of realistic models that include organic-inorganic composites. They later investigated Cs-, Na-, and Ca-hectorite with ^{133}Cs, ^{23}Na, and ^{43}Ca NMR to clarify the importance of the charge-balancing cation on the smectite [16]. The lower H_2O affinity and energy requirements for replacing water with CO_2 as a neighbor on Cs-hectorite compared to that with N^+ or Ca^{2+} eased the incorporation of CO_2 into the external surfaces and interlayers in the Cs analog, but dehydration of the interlayer was present in all cases of high pressure CO_2 to varying extents.

Other important considerations of geological carbon sequestration are the impact of supercritical CO_2 on the microbial populations beneath the surface and the ways

in which these populations influence carbon storage (prevent slipping of CO_2 or enhance mineral precipitation). Wilkins et al. studied how supercritical CO_2 exposure impacts the metabolism and stress response of a model sulfate-reducing bacterial strain [15]. *Desulfovibrio vulgaris* biomass was treated with ^{13}C–lactate prior to treatment with up to 80 bar of CO_2 in the HTHP rotors. The resulting ^{13}C HTHP NMR monitored the oxidation to ^{13}C-2-acetate and was consistent with the sulfide generation in that higher CO_2 pressures inhibited microbial activity. As seen in Fig. 2, oxidation of ^{13}C-3-lactate to acetate was monitored via the disappearance of lactate peaks at 4.04 and 1.26 ppm corresponding to CH and CH_3, respectively. Concurrent to this, the peak appearing at 1.84 ppm represents the acetate CH_3. At 1 bar CO_2 (A), 5 bar CO_2 (B), and 25 bar N_2 (D), complete conversion of lactate is observed over 5 h; however, at higher CO_2 pressures (C), incomplete lactate oxidation is present. This confirms the negative effect of CO_2 on microbial growth and respiration, since pressure alone does not account for the retarding phenomenon. This study highlighted the capability of HTHP MAS NMR to simulate natural environments for living organisms in order to gain fundamental insights into the chemical system impacting them.

In addition to mitigating anthropogenic carbon production, novel techniques of low-carbon energy alternatives by harnessing geothermal energy were studied using HTHP MAS NMR. Enhanced geothermal systems store fluid inside deep crystalline

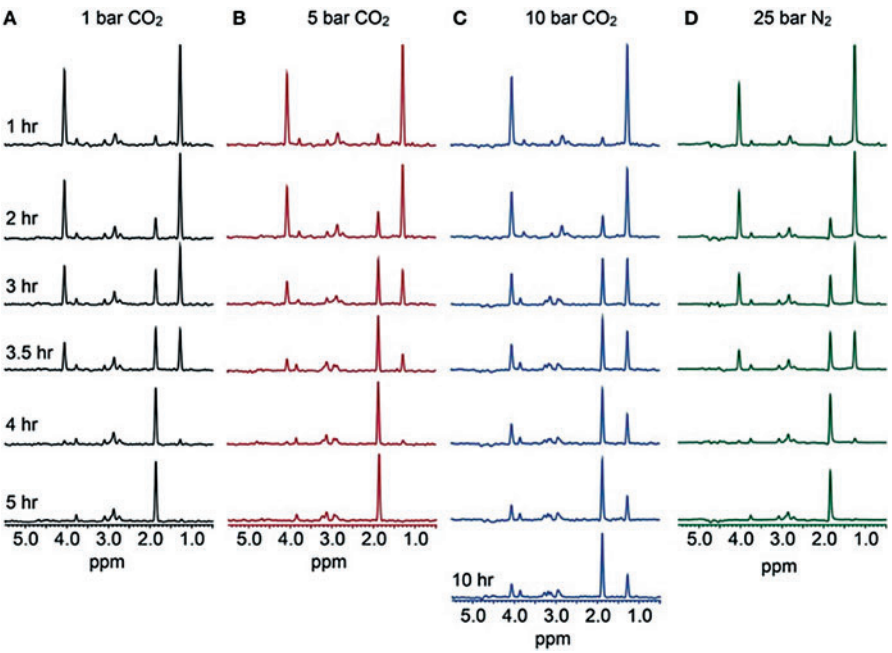

Fig. 2 NMR data collected over time as a function of rotor pressure monitoring the oxidation of ^{13}C-3-lactate to acetate at 1 bar CO_2 (**a**), 5 bar CO_2 (**b**), 10 bar CO_2 (**c**), and 25 bar N2 (**d**). Reprinted from Ref. [15] in accordance with Frontiers' copyright terms

bedrock where thermal energy can be drawn out. However, the challenges associated with the creation of safe, high-permeability reservoirs must be well understood and mitigated before the widespread application of such technologies in order to prevent adverse environmental impacts (such as the penetration of fracturing chemicals into aquifers). Jung et al. used the in situ HTHP technology to study a safe, CO_2-activated, rheoreversible fracturing fluid that enhances rock permeability at a significantly decreased level of effective stress [17]. In situ ^{13}C NMR provided confirmation of gel formation through speciation of CO_2 and the polyallylamine fluid up to 154 °C and 138 bar. The appearance of gel-related bicarbonate (158 ppm) and cross-linked urea (162 ppm) was noted. This validated the hypothesized interaction despite concerns that the gel would decompose at such high temperatures. High CO_2 pressures allowed the formation of carbonate species.

While the interaction of CO_2 in solid substrates has been a primary focus of the HTHP NMR in geochemistry, another greenhouse gas, methane, has recently been studied in an attempt to understand its behavior in nonporous and nanoporous minerals [18]. The authors in this study noted a change in the ^{13}C electronic environment relating to methane densification as the pressure was increased up to 130 bar with NMR. No change was observed with respect to temperature in the presence of fumed, nonporous silica or a pure methane phase; however, upon exposure to mesoporous silica, the chemical shift of methane split into two peaks due to the confining environment of the silica. When heated, only the confined methane species experienced a moderate upfield shift. This thermal effect was much more pronounced in matrices with a high content of mesoporous silica where the density of methane decreased with temperature. Both the confined and fluid phase methane responded to changes in pressure. In this observation, the densification was enhanced by pore confinement, leading to greater methane-methane interactions. This new insight paves the way for future studies on the role of pore size and how natural clays may exhibit similar properties.

Zeolite Catalysis: Dehydration, Alkylation, and Isomerization

Zeolites are highly utilized microporous aluminosilicate materials that are used ubiquitously everywhere from natural environments to chemical process facilities. Their tunable pore size and structure, along with their ability to incorporate a variety of cations, make them a flexible material for a variety of applications. Zeolites are heavily used in catalytic chemistry, where the protonated form can act as a solid-acid or additional metals can be incorporated to promote other chemistries. Recent applications of the HTHP rotors have probed organic reactions of renewable feedstocks over zeolitic materials for a more solid understanding of the reaction mechanisms involved in their catalytic transformations [10, 11, 19, 20]. In particular, dehydration, alkylation, and isomerization reactions of cyclic compounds were highlighted in those works.

A chief concern surrounding the appropriateness of labeling spectroscopic methods as relevant to standard conditions is how the materials respond in the

spectroscopy cell compared to normal operation. While the HTHP rotors indeed allow for investigation under more harsh conditions, it is important to demonstrate that the chemical transformations well-mimic those from outside the rotor, i.e., a standard batch reactor. In the case of a catalytic system, properties such as product selectivity and activation energy are great indicators of the rotor system exhibiting the same conditions as found in a batch reactor. This concern was evaluated using in situ ^{13}C HTHP MAS NMR to follow the dehydration of cyclohexanol catalyzed by phosphoric acid and also H-Beta zeolite [11]. In both cases, spectra were collected in the batch-like system over a period of time under varying temperature conditions. The turnover frequencies were plotted in an Arrhenius plot to provide the activation energy of each dehydration reaction. When compared to standard batch reactor data, good agreement was found in both the product distribution and the activation energies of H_3PO_4 and H-Beta catalyzed reactions where the activation energies for the HTHP rotors were 148 and 164 kJ/mol, respectively [11]. These results highlight the appropriateness of utilizing the HTHP rotors to collect in situ catalytic data in both homogeneous and heterogeneous systems.

Beyond simply analyzing the product composition and activation energy, the unique strengths of NMR can greatly aid in understanding the underlying mechanisms of the catalytic transformations. For instance, the hydrodeoxygenation of phenolic compounds requires an acid-functionalize catalyst to facilitate dehydration of intermediately formed cycloalkanols. Due to the two orders of magnitude higher zeolite-driven dehydration rate as compared to mineral acids, largely attributed to a stabilizing confinement effect, the heterogeneous route is of greater interest [21]. A closer examination of the data collected for cyclohexanol dehydration over H-Beta zeolite reveals a deeper awareness of the molecular picture of this reaction. E1 mechanisms had been previously suggested for aqueous phase mineral acid dehydration as well as gas phase over polyoxometalates and zeolites [22, 23]. To expose the heterogeneous reaction mechanism of cyclohexanol dehydration over H-Beta in water, reaction data were collected in the HTHP rotor over a period of 23 h at 130 °C [10]. The results can be seen in Fig. 3.

Initially, 1-^{13}C-cyclohexanol was seen as a narrow peak resonating at 70 ppm, corresponding to the aqueous phase. A relatively broad peak was also present at 70.8 ppm, suggesting that approximately 50% of the cyclohexanol was adsorbed in the pores of H-Beta. It follows that cyclohexanol only occupied about one quarter of the total pore volume, but this was still a remarkable enhancement (20-fold) as compared to the aqueous phase reaction. The formation of cyclohexene and dicyclohexyl ether was initially observed, with isotopic scrambling of the labeled ^{13}C throughout the alicyclic ring. Cyclohexyl-1-cyclohexene makes an appearance as a secondary product at later times. A mechanistic clarification was made possible by modeling the initial rates with a kinetic model. The proposed model fit the data well and suggested an E1-type mechanism proceeding through a carbenium ion. The cyclohexyl cation underwent a 1,2-hydride shift that competes with rehydration and deprotonation. As equilibrium was established, the cyclohexyl carbenium ion becomes more likely to interact with cyclohexene in an electrophilic attack to form the cyclohexyl-1-cyclohexene seen later in the NMR spectra.

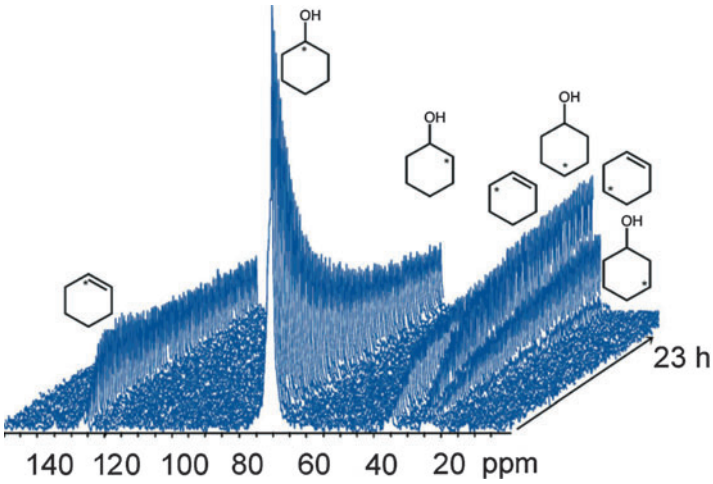

Fig. 3 Stacked plot containing 80 MAS NMR spectra acquired for a mixture of 22 mg HBEA150 and 120 uL of 0.33 M 1-^{13}C-cylohexanol at 120 °C in liquid water and as a function of time. Reprinted from Ref. [10] with permission from John Wiley & Sons

The proposed mechanism derived by the HTHP rotors differs from those speculated in the absence of water, where a surface-bound alkoxide species is formed [24]. This species was not observed in any of the collected ^{13}C NMR data, suggesting a different mechanism in the presence of water. The authors make it clear that the E2 pathway holds no relevance for the studied system, where the initial rate of cyclohexanol disappearance would be equivalent to the cyclohexene appearance. Instead, the disappearance is 2.5 times the formation rate of 1-^{13}C-cyclohexene. Formation rates of the 2-^{13}C and 3-^{13}C analogs are 5 and 10 times the disappearance of 1-^{13}C-cyclohexanol, respectively. As such, the E1 mechanism was validated by numerous key pieces of evidence derived from in situ NMR.

A subsequent study on the phenol alkylation on H-beta zeolite in decalin probed the transformation of cyclohexanol further [20]. This reaction serves as an important model for the catalytic conversion of lignin-derived compounds obtained from lignocellulosic biomass, which are heavily used in gasolines, lubricants, and commodity chemicals. Phenol alkylation is known to proceed via an electrophilic aromatic substitution where the formed carbenium ion serves as the electrophile. The proposed mechanisms for the alkylation of phenol are largely based on Friedel-Crafts chemistry in the homogeneous phase or contrasting theoretical predictions instead of rigorous rate or spectroscopic analysis, especially in the case of an alcohol-based alkylating agent. To highlight the relevant interactions occurring at the interface and clarify the mechanistic expression, a batch reactor undergoing phenol alkylation with cyclohexanol was simulated with HTHP rotors at temperatures up to 142 °C [20].

To better understand the reaction dynamics, variable temperature experiments were conducted with both phenol and cyclohexanol individually. The collected

spectra each harbored a narrow peak (156.3 ppm and 69.8 ppm, respectively) attributed to the mobile phase and broad peaks (155.5 ppm and 71.6 ppm, respectively) that paralleled theoretical predictions of the adsorbed molecules. Both compounds exhibited exothermic adsorption based upon the increase in the relative peak areas of the mobile phase as the temperature increased. Uptake values were calculated and shown to be an order of magnitude greater than the Brønsted acid content, suggesting that most of the organic molecules were physisorbed in the pores and not interacting directly with the acid site. Since the molar ratios of adsorbed and mobile molecules were similar for the two molecules across the temperature range investigated, it was speculated that they would exhibit similar enthalpies of adsorption on H-BEA, where adsorption constants at 25 °C were measured as 44 and 73, respectively.

As evidenced by the four plots in Fig. 4a–d, the initial in situ reaction data demonstrated the presence of only cyclohexanol dehydration to 1-^{13}C-cyclohexne (and the formation of small quantities of isotopomers at longer residence times) over the first 400 min. Around this time, a weak signal at 74.8 ppm ascribed to dicyclohexyl ether was observed and disappeared quickly. It was not until a majority of the cyclohexanol had dehydrated to cyclohexene that the rate of phenol alkylation increased. After this 400-min mark, the 1-^{13}C-phenol signal decreased and gave way to cyclohexyl phenyl ether, 4- and 2-cyclohexylphenol, and 2,4-dicylohexylphenol. The cyclohexyl phenyl ether reached a maximum concentration at 600 min before reducing in spectral intensity as the C-alkylation products continued to be produced throughout the duration of the experiment (Fig. 4), demonstrating the greater stability of C-alkylation products compared to *O*-alkylation products. Ortho substitution occurred at a greater frequency than para substitution (Fig. 4d). This selectivity effect was attributed to the pore constrains of H-Beta. The data clearly indicates some competitive adsorption behavior is afoot between either the phenol or alkylating agent and cyclohexanol. Though the adsorption thermodynamics of the two reactants are similar, the specific role cyclohexanol's dehydration was poorly understood. To probe the unexpected behavior of the delayed alkylation, experiments were conducted in the same work to assess the roles of cyclohexanol and cyclohexene.

When 1-^{13}C-phenol was added with cyclohexene into the HTHP rotors for in situ analysis, the phenol concentration was spectroscopically observed to decrease exponentially as time progressed. Identical product distribution trends to those in the cyclohexanol reaction after 400 min were observed with this experiment with the exception of the more rapid development of dialkylation (2,4-dicyclohexylphenol). When the experiment was repeated with the inclusion of cyclohexanol, the reaction rate was severely arrested until a significant fraction of the cyclohexanol had been dehydrated. This observation requires that the alkylating agent is not generated as a dehydration intermediate and that its generation is in direct competition with the presence of cyclohexanol. Zhao et al. noted that the formation of isotopomers of cyclohexene were observed well after the initial stages of cycloalkanol dehydration, and became randomly distributed in the alkylation products after 700 min of residence time. This result suggests that cyclohexene readsorbs and is protonated

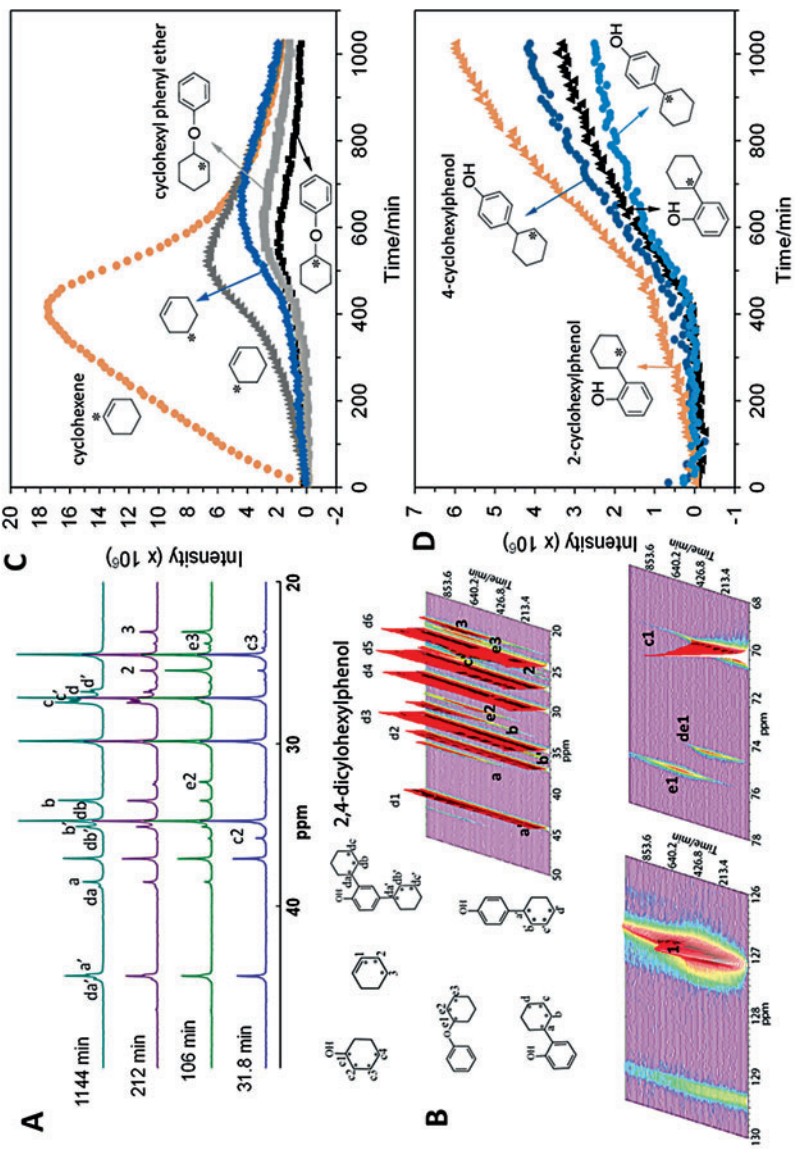

Fig. 4 Collected data from the in situ NMR investigation of phenol-cyclohexanol alkylation catalyzed by H-BEA in decalin (unlabeled) at 127 °C, including (**a**) vertically stacked spectral plots of the ^{13}C aliphatic region as a function of time, (**b**) stack-plot of the ^{13}C signals a function of time, (**c**) quantitative analysis of dehydration products as a function of time, and (**d**) quantitative analysis of ortho- and para-C-alkylation products as a function of time. The ^{13}C positions are identified on the structures for the chemical species observed. Adapted from the Ref. [20]. Copyright 2017 American Chemical Society

at the acid site to form the carbenium ion, facilitating both the production of the alkylating agent and isotopic scrambling. The favorability (nearly double) of 2-^{13}C-cyclohexylphenol alkylation products over 1-^{13}C-cyclohexylphenol in both ortho- and para- substituted alkylation products (Fig. 4d) also played an important role in describing the reaction mechanism. If phenol reacted with an intermediate generated by cyclohexanol dehydration, even in the case of a rapid hydride shift, a majority of the product should be the 1-^{13}C-cyclohexylphenol. Consequently, the lack of carbenium ion formation during the dehydration of cyclohexanol suggests that E2 chemistry drives the first step of dimer dehydration, unlike what was noted in the aqueous phase. Zhao et al. conclude that phenol alkylation with cyclohexanol on H-BEA in decalin occurs primarily via a rapid electrophilic attack by a cyclohexyl cation generated by the readsorption of cyclohexene after a sufficient quantity of cyclohexanol has been exhausted. This unique and detailed isotopic insight is a distinct advantage that in situ HPHT MAS NMR can provide in assessing reaction pathways over traditional methods.

Another recent application of the HTHP rotor technologies was the revelation of the solvent effects of biomass isomerization. In this study by Qi et al., the glucose isomerization rate over NaX and NaY zeolites was noted to decrease dramatically when cosolvent γ-valerolactone (GVL) was added to water in small quantities, and recovered as the concentration increased up to 62% of the water-only value [19]. This observation was in contrast to what had been observed in the homogeneous isomerization where the incorporation of GVL promoted activity up to the glucose solubility limit of 46%. To probe this effect, *operando* measurements were performed at 130 °C, noting the concentrations of substrate and products and the effect of solvent on the adsorption of glucose.

Qi et al. found that the presence of a small amount of organic cosolvent suppressed glucose adsorption on the zeolite as GVL was favored to interact with the active site. Upon increasing the content of cosolvent, a simultaneous increase in water and glucose in the adsorbed phase was observed, where the glucose concentration exceeded 30 times the value in the pure water system at the maximum GVL content. This increase in water and glucose uptake was explained by the preferential adsorption of these molecules by the zeolite relative to the GVL-rich liquid phase where enhanced hydrophobicity arose. This specific application demonstrated the usefulness of HTHP NMR in evaluating the specific solvent effects of liquid-phase heterogeneous reactions. More broadly, the high-temperature, high-pressure technology has helped discern the underlying reaction mechanisms of reactions occurring under elevated conditions. This will become a more important tool for catalytic scientists as the methods and technology continue to progress.

Materials Synthesis

Similar in nature to zeolites, microporous aluminophosphate materials serve an important role as molecular sieves in catalysis, separations, ion exchange, and gas

storage. Copious structural variations have been employed for various processes, but diversification primarily arose from trial and error synthesis strategies where little insight on the crystallization mechanism was available. Though essential information for engineering-tunable synthesis methods, a clear molecular picture of the crystallization process for these materials is complicated by the high-temperature, high-pressure nature of the synthesis conditions promoting phase transformations. These crystallization processes usually occur in a sealed autoclave at elevated temperatures for extended periods of times. For these systems, NMR is uniquely suitable to elucidate the role of water during synthesis and provide discrete insight on the local structure of organic and inorganic species as well as their interactions. Investigation by traditional NMR is limited only to those cases where relatively low temperatures are used for synthesis [25]. For instances in which synthesis temperatures exceed 100 °C HTHP rotors will be essential for in situ investigation. Two relevant studies have reported the use of HTHP NMR to understand the synthesis of $AlPO_4$–5 and the subsequent crystallization to the dense phase $AlPO_4$-tridymite [26, 27].

Initial studies on the synthesis of $AlPO_4$–5 have noted that the aluminophosphate network arises from poorly ordered Al-O-P chains that crystallized into the channel structure through potential intermediate phases [28–32]. The generality of the observations encumbered a clear depiction of the structural reorganization at the molecular level. In situ ^{27}Al, ^{31}P, ^{13}C, and ^{1}H NMR were conducted with HTHP rotors to better understand the crystallization of $AlPO_4$–5 and the role water plays in its formation [27]. The synthesis gel was probed at various steps along heating and over time after reaching the desired temperature of 150 °C. Zhao et al. observed the six-coordinated $Al(OP)_4(H_2O)_2$ ^{27}Al signal transform into the $Al(OP)_4$ species by the elimination of water, evidenced by concomitant formation of a liquid phase at 4.5 ppm in ^{1}H and enhanced shielding of the ^{31}P signal. The authors also detected cross-linking between phosphate and aluminum during heating based on an increase in condensed P species observed at higher temperatures and an upfield shift of the four-coordinated aluminum sites. The sharp water peak was no longer observed at 150 °C due to fast exchange with the broad ^{1}H species, signaling high-mobility at high temperature.

The reaction was observed over time by NMR in a HTHP rotor at reaction conditions, see Fig. 5. The ^{27}Al spectra, Fig. 5a, show a gradual narrowing of the four-coordinated species (37 ppm) and a shift upfield, which is attributed to framework $AlPO_4$–5. A narrow peak at 46 ppm also formed, which was identified as five-coordinated Al bonded to HPO_4^{-2} ions in the synthesis solution. Octahedral species were also observed (12 ppm). The ^{31}P spectra, Fig. 5b, clearly depicts the broadening of the terminal phosphate at −8 ppm as a shoulder develops downfield, suggesting the replacement of Al-O-P linkages for terminal phosphates. The peaks merged as the exchange between varying aluminum phosphate complexes took place and demonstrated oscillatory behavior as a repeated hydrolysis and condensation reaction occurred during terminal phosphates production and consumption. Additionally, four new ^{31}P peaks developed at −16, −19, −24, and −29 ppm showing the

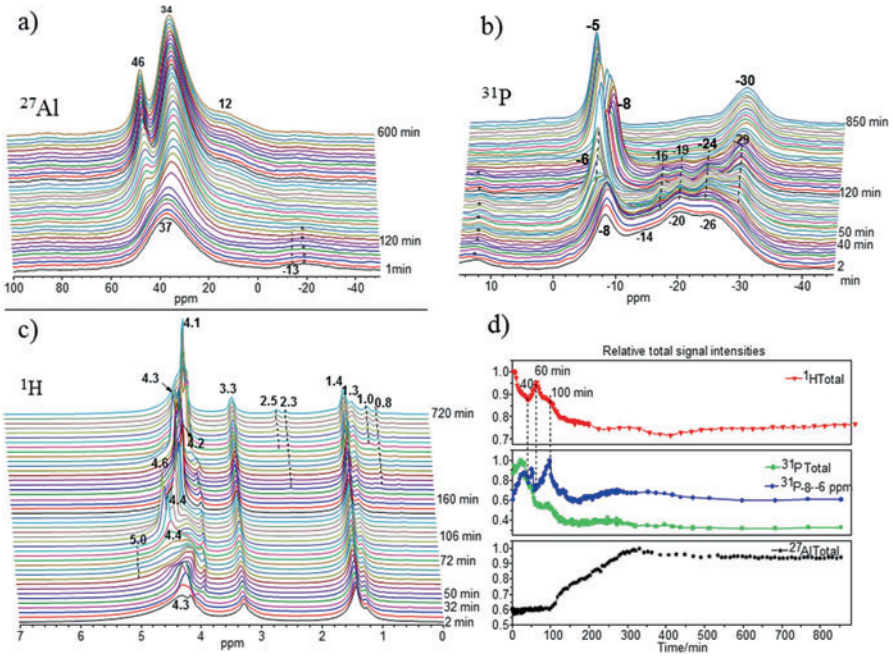

Fig. 5 Time on stream in situ MAS NMR spectra and their relative signal intensities of synthesis gel crystallized at 150 °C: (**a**) ^{27}Al, (**b**) ^{31}P, (**c**) ^{1}H MAS NMR, and (**d**) normalized signal intensities. Adapted from Ref. [27]. Copyright 2016 American Chemical Society

formation of several short-range ordered structures. The first three of these peaks disappeared as crystallization progressed and a major peak at −30 ppm prevailed, corresponding to framework P in $AlPO_4$–5.

Proton NMR displayed no significant change in organic template peaks (1.4 and 3.3 ppm) except a slight narrowing during crystallization; however, many changes did occur downfield. As the synthesis progressed, the peaks associated with hydroxyl groups, protonated amines, and water narrowed due to enhanced exchange. The spectra show that water indeed plays an important role during the process by catalyzing the hydrolysis of the Al-O-P bonds. The peak at 5 ppm supports the concept that the hydrogen bond interaction between the template and phosphate facilitates the organization of the channeled structure. The formation of liquid water was quite clear and the peak position fluctuated with pH as a downfield movement coincided with the release of excess phosphate in the gel and upfield as it was consumed during crystal growth.

The use of the HTHP rotors enabled for a much clearer picture of the oscillating crystallization of the amorphous gel into $AlPO_4$–5, especially in regards to clarifying the catalytic role of water during the nucleation period by facilitating hydrolysis and condensation. Investigation of this system also extended into the phase transformation of $AlPO_4$–5 to the more stable $AlPO_4$-tridymite upon posttreatment of the

aluminophosphate [26]. This phase transformation takes place as $AlPO_4$–5 is again heated at 150 °C under pressure in the presence of water for an extended time, an ideal system for investigation with the HTHP rotors.

Xu et al. showed a strong growth narrowing of the ^{27}Al signal and dramatic rise in side bands after 7 h of exposure, demonstrating that $AlPO_4$-tridymite had formed. It was found that this peak was due to residual amorphous aluminophosphate, as the original peak was unaltered and overlapping with the new one. With prolonged heating, the broad peak of $AlPO_4$–5 does diminish to yield the more stable species. This transition was nearly completed after 20 h. They also used ^{31}P HTHP MAS NMR to demonstrate the transition of dissolved phosphate species to terminal phosphates after 2 h. Concurrently, the amorphous species are shown to decrease, consistent with ^{27}Al data. The terminal phosphate species decreased after about 7 h, where the $AlPO_4$-tridymite species arose as the amorphous phase crystallizes. The phosphorous signal also demonstrated the late transformation of $AlPO_4$–5 to the more stable phase. Proton NMR played a role in deciphering the mechanism of this transformation by the strong hydrogen bonding between protonated amines and aluminophosphates exchanging with water. This peak shifted downfield over the first few hours while a new peak attributed also to protonated amines appeared at 5.2 ppm and shifted to 6.2 ppm. Condensation reactions were witnessed initially by the increase of water signal and concurring decrease in hydroxyl signal. After about 7 h, the water signal dispersed into many environments as hydrolysis and condensation reactions reformed the aluminophosphate. After 9 h, the bulk water signal returned as it was released from the gel in the formation of crystalline $AlPO_4$-tridymite, facilitating dissolution of aluminophosphate complexes. Relatively few additional changes were noted in the spectra, but HTHP NMR played an essential role in better understanding the steps and mechanisms involved in this posttreatment. Clearly, the ability to probe materials during synthesis can lead to a broader understanding of the materials generated, potentially leading to highly tunable synthesis procedures. In cases where high temperatures and pressures are utilized in materials formation, HTHP MAS NMR will play an important role in describing the chemical interactions.

Conclusion

The recent advancement of high-pressure, high-temperature MAS NMR systems has seen a dramatic improvement over the previous methods of glass and polymer rotors and their notable drawbacks. The advent of reusable, sealable ceramic NMR rotors capable of operating at high temperatures and pressures while spinning at a suitable rate has greatly expanded the systems for which NMR can provide useful data. This high-resolution, *operando* MAS NMR capability has already demonstrated great use in the field of geochemistry where the sequestration of carbon in minerals has been investigated alongside the confinement of methane and impact of factorization fluids on biological specimens in the minerals with in situ reaction data. The field of catalysis has also seen notable benefit in the enhanced description of organic cyclic

compounds for which rate data matches well with reaction-generated data, and new insight on the reaction mechanisms has been made available. Lastly, new fundamental insights on the mechanisms of materials synthesis have been brought about by the use of the HTHP rotors. The combined advantages of exposing a system to its natural conditions and probing the nuclei as the interactions take place make the in situ HTHP MAS NMR a powerful tool for studying interaction dynamics and reaction pathways of chemical systems that will continue to be useful as the technology matures.

References

1. Andrew ER, Bradbury A, Eades RG. Nuclear Magnetic Resonance Spectra from a Crystal rotated at High Speed. Nature. 1958;182:1659.
2. Lowe IJ. Free Induction Decays of Rotating Solids. Phys Rev Lett. 1959;2:285–7.
3. Miyoshi T, Takegoshi K, Terao T. ^{13}C High-Pressure CPMAS NMR Characterization of the Molecular Motion of Polystyrene Plasticized by CO_2 Gas. Macromolecules. 1997;30:6582–5.
4. Miyoshi T, Takegoshi K, Terao T. ^{129}Xe n.m.r. study of free volume and phase separation of the polystyrene/poly(vinyl methyl ether) blend. Polymer. 1997;38:5475–80.
5. Miyoshi T, Takegoshi K, Terao T. Effects of Xe Gas on Segmental Motion in a Polymer Blend As Studied by ^{13}C and ^{129}Xe High-Pressure MAS NMR. Macromolecules. 2002;35:151–4.
6. Yonker CR, Linehan JC. The use of supercritical fluids as solvents for NMR spectroscopy. Prog Nucl Magn Reson Spectrosc. 2005;47:95–109.
7. Deuchande T, Breton O, Haedelt J, Hughes E. Design and performance of a high pressure insert for use in a standard magic angle spinning NMR probe. J Magn Reson. 2006;183:178–82.
8. Hoyt DW, Turcu RVF, Sears JA, Rosso KM, Burton SD, Felmy AR, et al. High-pressure magic angle spinning nuclear magnetic resonance. J Magn Reson. 2011;212:378–85.
9. Turcu RVF, Hoyt DW, Rosso KM, Sears JA, Loring JS, Felmy AR, et al. Rotor design for high pressure magic angle spinning nuclear magnetic resonance. J Magn Reson. 2013;226:64–9.
10. Vjunov A, Hu MY, Feng J, Camaioni DM, Mei D, Hu JZ, et al. Following solid-acid-catalyzed reactions by MAS NMR spectroscopy in liquid phase – zeolite-catalyzed conversion of cyclohexanol in water. Angew Chem Int Ed. 2014;53:479–82.
11. Hu JZ, Hu MY, Zhao Z, Xu S, Vjunov A, Shi H, et al. Sealed rotors for in situ high temperature high pressure MAS NMR. Chem Commun. 2015;51:13458–61.
12. Loring JS, Schaef HT, Turcu RVF, Thompson CJ, Miller QRS, Martin PF, et al. In Situ Molecular Spectroscopic Evidence for CO_2 Intercalation into Montmorillonite in Supercritical Carbon Dioxide. Langmuir. 2012;28:7125–8.
13. Miller QRS, Thompson CJ, Loring JS, Windisch CF, Bowden ME, Hoyt DW, et al. Insights into silicate carbonation processes in water-bearing supercritical CO_2 fluids. Int J Greenhouse Gas Control. 2013;15:104–18.
14. Bowers GM, Hoyt DW, Burton SD, Ferguson BO, Varga T, Kirkpatrick RJ. In Situ ^{13}C and ^{23}Na Magic Angle Spinning NMR Investigation of Supercritical CO_2 Incorporation in Smectite–Natural Organic Matter Composites. J Phys Chem C. 2014;118:3564–73.
15. Wilkins MJ, Hoyt DW, Marshall MJ, Alderson PA, Plymale AE, Markillie LM, et al. CO_2 exposure at pressure impacts metabolism and stress responses in the model sulfate-reducing bacterium *Desulfovibrio vulgaris* strain Hildenborough. Front Microbiol. 2014;5:507.
16. Bowers GM, Schaef HT, Loring JS, Hoyt DW, Burton SD, Walter ED, et al. Role of Cations in CO_2 Adsorption, Dynamics, and Hydration in Smectite Clays under in Situ Supercritical CO_2 Conditions. J Phys Chem C. 2017;121:577–92.

17. Jung HB, Carroll KC, Kabilan S, Heldebrant DJ, Hoyt D, Zhong L, et al. Stimuli-responsive/rheoreversible hydraulic fracturing fluids as a greener alternative to support geothermal and fossil energy production. Green Chem. 2015;17:2799–812.
18. Ok S, Hoyt DW, Andersen A, Sheets J, Welch SA, Cole DR, et al. Surface Interactions and Confinement of Methane: A High Pressure Magic Angle Spinning NMR and Computational Chemistry Study. Langmuir. 2017;33:1359–67.
19. Qi L, Alamillo R, Elliott WA, Andersen A, Hoyt DW, Walter ED, et al. Operando Solid-State NMR Observation of Solvent-Mediated Adsorption-Reaction of Carbohydrates in Zeolites. ACS Catal. 2017;7:3489–500.
20. Zhao Z, Shi H, Wan C, Hu MY, Liu Y, Mei D, et al. Mechanism of phenol alkylation in zeolite H-BEA using in situ solid-state NMR spectroscopy. J Am Chem Soc. 2017;139:9178–85.
21. Zhao C, Lercher JA. Selective Hydrodeoxygenation of Lignin-Derived Phenolic Monomers and Dimers to Cycloalkanes on Pd/C and HZSM-5 Catalysts. ChemCatChem. 2012;4:64–8.
22. Corma A, Garcia H. Organic reactions catalyzed over solid acids. Catal Today. 1997;38:257–308.
23. Janik MJ, Macht J, Iglesia E, Neurock M. Correlating Acid Properties and Catalytic Function: A First-Principles Analysis of Alcohol Dehydration Pathways on Polyoxometalates. J Phys Chem C. 2009;113:1872–85.
24. Chiang H, Bhan A. Catalytic consequences of hydroxyl group location on the rate and mechanism of parallel dehydration reactions of ethanol over acidic zeolites. J Catal. 2010;271:251–61.
25. Aerts A, Kirschhock CEA, Martens JA. Methods for in situ spectroscopic probing of the synthesis of a zeolite. Chem Soc Rev. 2010;39:4626–42.
26. Xu S, Zhao Z, Hu MY, Han X, Hu JZ, Bao X. Investigation of water assisted phase transformation process from AlPO4-5 to AlPO4-tridymite. Microporous and Mesoporous Materials. 2016;223:241-6.
27. Zhao Z, Xu S, Hu MY, Bao X, Hu JZ. In situ high temperature high pressure MAS NMR study on the crystallization of AlPO4-5. J Phys Chem C. 2016;120:1701–8.
28. Rey F, Sankar G, Thomas JM, Barrett PA, Lewis DW, Catlow CRA, et al. Greaves, Synchrotron-Based Method for the Study of Crystallization: Templated Formation of CoALPO-5 Catalyst. Chem Mater. 1995;7:1435–6.
29. Grandjean D, Beale AM, Petukhov AV, Weckhuysen BM. Unraveling the Crystallization Mechanism of CoAPO-5 Molecular Sieves under Hydrothermal Conditions. J Am Chem Soc. 2005;127:14454–65.
30. Longstaffe JG, Chen B, Huang Y. Characterization of the amorphous phases formed during the synthesis of microporous material AlPO4-5. Microporous Mesoporous Mater. 2007;98:21–8.
31. Xu J, Chen L, Zeng D, Yang J, Zhang M, Ye C, et al. Crystallization of AlPO4-5 Aluminophosphate Molecular Sieve Prepared in Fluoride Medium: A Multinuclear Solid-State NMR Study. J Phys Chem B. 2007;111:7105–13.
32. Fan F, Feng Z, Sun K, Guo M, Guo Q, Song Y, et al. In Situ UV Raman Spectroscopic Study on the Synthesis Mechanism of AlPO-5. Angew Chem. 2009;121:8899–903.